

Anomalous Evolution of Strength and Microstructure of High-Entropy Alloy CoCrFeNiMn after High-Pressure Torsion at 300 and 77 K

Aleksey V. Podolskiy, Yuriy O. Shapovalov, Elena D. Tabachnikova, Aleksandr S. Tortika, Mikhail A. Tikhonovsky, Bertalan Joni, Eva Ódor, Tamas Ungar, Stefan Maier, Christian Rentenberger, Michael J. Zehetbauer,* and Erhard Schafner

Ultrafine and nanocrystalline states of equiatomic face-centered cubic (fcc) high-entropy alloy (HEA) CoCrFeNiMn (“Cantor” alloy) are achieved by high-pressure torsion (HPT) at 300 K (room temperature, RT) and 77 K (cryo). Although the hardness after RT-HPT reaches exceptionally high values, those from cryo-HPT are distinctly lower, at least when the torsional strain lies beyond $\gamma = 25$. The values are stable even during long-time storage at ambient temperature. A similar paradoxical result is reflected by torque data measured in situ during HPT processing. The reasons for this paradox are attributed to the enhanced hydrostatic pressure, cryogenic temperature, and especially large shear strains achieved by the cryo-HPT. At these conditions, selected area electron diffraction (SAD) patterns indicate that a partial local phase change from fcc to hexagonal close-packed (hcp) structure occurs, which results in a highly heterogeneous structure. This heterogeneity is accompanied by both an increase in average grain size and especially a strong decrease in average dislocation density, which is estimated to mainly cause the paradox low strength.

conventional alloys, those alloys reach high values of entropy of mixing and have thus been called “high-entropy alloys (HEAs)”. HEAs usually have face-centered cubic (fcc) or body-centered cubic (bcc) crystal structures and show advanced mechanical properties, which means high strength accompanied by reasonable plasticity.^[15,16] From usual metals and alloys, it is known that further improvements in strength and plasticity may be reached by introducing an ultrafine-grained or nanocrystalline state.^[19] So far, grain refinement in HEAs was achieved by different kinds of plastic deformation such as hot forging,^[20] rolling,^[21,22] and friction stir processing.^[23] Recently, a nanocrystalline state was produced in the single-phase HEA with components CoCrFeNiMn (the “Cantor alloy”^[2] in case of equiatomic alloy) by high-pressure torsion (HPT) at ambient temper-


ature^[24–35]; it was shown by tension experiments done at 300 K that the HPT-induced transition to nanocrystalline structure allows a significant increase of the strength while retaining the plasticity. It was shown earlier for conventional metals^[36,37] that additional improvements of mechanical characteristics can be achieved by decreasing the processing temperature of HPT to cryogenic regions. From HEAs, the Cantor alloy exhibits

1. Introduction

For a long time, crystalline alloys based on one to three components and comparable parts were used for production of high-strength materials; in recent years, however, principally new alloys were developed containing at least five elements in nearly equal concentrations of about 5–35 at%.^[1–18] In comparison to

Dr. A. V. Podolskiy, Y. O. Shapovalov, Dr. E. D. Tabachnikova
B. Verkin Institute for Low Temperature Physics & Engineering
47 Nauky Ave., Kharkov 61103, Ukraine

A. S. Tortika, Dr. M. A. Tikhonovsky
National Science Center
Kharkov Institute of Physics and Technology
1 Akademicheskaya Str, Kharkov 61108, Ukraine

 The ORCID identification number(s) for the author(s) of this article can be found under <https://doi.org/10.1002/adem.201900752>.

© 2019 The Authors. Published by WILEY-VCH Verlag GmbH & Co. KGaA, Weinheim. This is an open access article under the terms of the Creative Commons Attribution-NonCommercial-NoDerivs License, which permits use and distribution in any medium, provided the original work is properly cited, the use is non-commercial and no modifications or adaptations are made.

DOI: 10.1002/adem.201900752

B. Joni, E. Ódor, Prof. T. Ungar
Department of Materials Physics
Eötvös Lorand University Budapest
Pazmany Peter setany 1/a, H-1117 Budapest, Hungary

Prof. T. Ungar
School of Materials
The University of Manchester
Manchester M13 9PL, UK

S. Maier, Prof. C. Rentenberger, Prof. M. J. Zehetbauer, Prof. E. Schafner
Physics of Nanostructured Materials
Faculty of Physics
University of Vienna
Boltzmannngasse 5, Vienna A-1090, Austria
E-mail: michael.zehetbauer@univie.ac.at

interesting properties at cryogenic temperatures, such as high cryogenic strength^[11] and high cryogenic toughness^[7] that is already in its coarse-grained state. Regarding fine- and ultrafine-grained states, only a few works performed cryo-HPT processing at 77 K with the goal of achieving ultrafine-grained or even nanocrystalline structures^[26,29,30,33,34] and having done cryo-rolling.^[22] Again, unusual effects occurred with the cryogenic HPT-processed materials at least with von Mises equivalent true strains >100 and hydrostatic pressures higher than 1 GPa showing a distinctly lower strength than that of the HPT RT-processed materials. In summary, all these investigations promise exceptional mechanical properties of the CoCrFeNiMn alloy in its nanocrystalline state for the ambient and especially in the cryogenic range of testing temperatures, which are therefore in focus in the present work.

2. Experimental Section

The ingots of equiatomic fcc HEA CoCrFeNiMn (Cantor alloy) were produced by arc melting of the components in high-purity argon inside a water-cooled copper cavity. The purities of the alloying elements were better than 99.9%. To ensure chemical homogeneity, the ingots were flipped over and remelted at least five times. Afterward, homogenization was achieved at 1000 °C for 24 h (in vacuum), which was followed by rolling from 5.3 to 2 mm, by annealing at 800 °C (1 h), another rolling from 2 to 1 mm, and further annealing at 1000 °C (1 h). The average grain size after this treatment amounted to 4 μm. Detailed characterization of the initial microstructure was done in numerous works.^[7,11,22] A careful X-ray diffraction study using a high-intense beam of rotating anode (see later) exhibited an fcc-type solid solution (Figure 1).

Severe plastic deformation of the alloy was performed using HPT. Disc-shaped billets with diameter 10 mm and thickness 0.9 mm were processed by five revolutions and a hydrostatic pressure of 6 GPa (a few tests were also done at 4 and 8 GPa) and at processing temperatures of 300 and 77 K. Values of shear (torsional) strain have been calculated by using the equation $\gamma = 2\pi n r/h$, where n is the number of rotations, r is the distance from rotation axis, and h is the sample thickness achieved after HPT processing. The temperature of 77 K was achieved by merging the sample and HPT plungers into liquid nitrogen. The plungers have been rotated by a speed of 0.2 rotations min^{-1} , corresponding to a maximum torsional shear strain rate $d\gamma/dt = 1.1 \times 10^{-1} \text{ s}^{-1}$. Straight radial lines have been attached to the upper and lower surfaces of samples, which could also be identified after the HPT processing, and the rotation angle fully coincided with the monitored rotations of the plunger, indicating that no slip occurred during HPT processing; moreover, such a slip event would have manifested in a sudden decrease in the torque curves, but such decreases were never observed (Figure 2a).

The in situ torques during the HPT process were measured by two V-shaped strain gauges connected as full bridges. These strain gauges were diagonally arranged on a hollow cylinder made of steel supporting the nonrotating, fixed HPT anvil, being part of the HPT facility used. After appropriate calibration, the nominal electronic torque resolution was 0.01 Nm, whereas

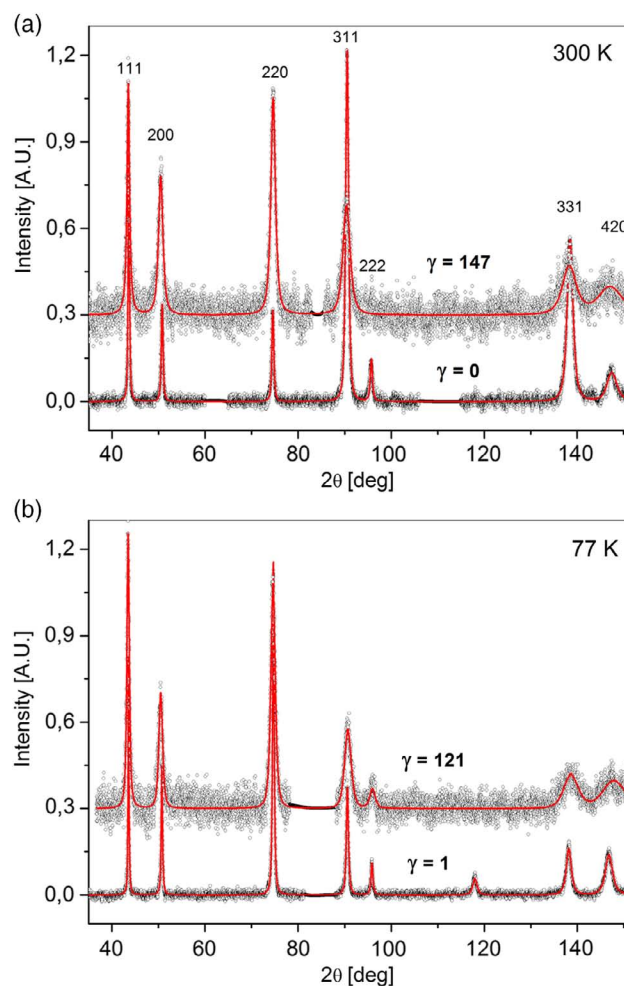


Figure 1. X-ray diffraction patterns of HEA “Cantor alloy” a) before and after RT-HPT processing, and b) after cryo-HPT processing. The HPT processing was done at a pressure of 6 GPa and till a torsional shear strain γ as indicated. All Bragg peaks indicate a solid-solution fcc lattice and show extensive broadening from both dislocations and limited crystallite sizes.

the electronic measuring noise was about a factor 10 higher. For the shear stress derived, this means a measuring resolution of distinctly below 1 MPa. The torsional shear stress was calculated by means of the formula $\tau = 3Q/(2\pi r^3)$ with Q as the torque and r as the radius of the HPT disc.

The microstructure of the HPT samples was studied using a Philips CM200 transmission electron microscope operated at 200 kV. For the transmission electron microscopy (TEM) investigations, the discs were electropolished until perforation using an electrolyte consisting of 95% $\text{C}_2\text{H}_5\text{OH}$ and 5% HClO_4 . By means of the selected area diffraction (SAD), the electron diffraction patterns from sample areas as small as 1.2 μm could be achieved. Diffraction intensity profiles were calculated by integration along the diffraction rings using the PASAD tools.^[38] Samples for the scanning electron microscopy (SEM) were grinded by SiC papers with 600 and 1200 grids, later polished by Al_2O_3 powders with particle sizes 1 and 0.3 μm. The polished surfaces have been investigated in the back-scattered

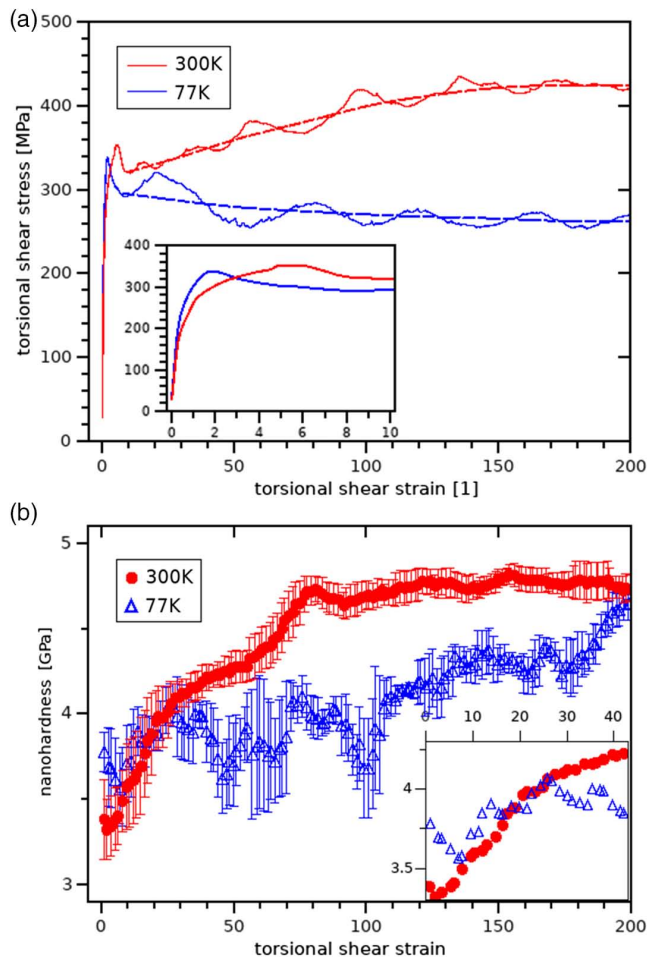


Figure 2. a) Torsional shear stress as derived from the torque data measured in situ during RT-HPT processing and cryo-HPT. The wavy behavior occurs in periods of full rotations and thus indicates the misalignment of torsional axis of HPT setup. The dashed lines denote the averaged curves as a guide for the eye. The insert enlarges the low-strain range of torque data and shows a cross-over of shear stress curves taken at 300 and 77 K, respectively. b) Nanohardness as a function of torsional shear strain also showing values of cryo-HPT processing being distinctly lower than those of RT processing, at least for torsional shears strains $\gamma < 200$ but higher than $\gamma \approx 20$ where a cross-over of nanohardness data occurs. The latter is demonstrated in more detail by the inset.

electron (BSE) modus. The investigations were conducted using FEG-SEM ZEISS SUPRA 55 V operated at 20 kV.

The X-ray diffraction measurements were performed on a special high-resolution diffractometer with a Ge (220) primary monochromator attached to a Cu $K\alpha$ fine-focus-rotating Cu anode (Rigaku MultiMax-9) operating at 40 kV and 100 mA. The beam had a size of about 0.2×1.5 mm on the specimen surface. The diffraction patterns were derived from integration of the intensities along Debye-Scherrer ring fragments obtained from two curved imaging plates (IPs) with a linear spatial resolution of 50 μm . The distances between the specimen and detector were selected such that the instrumental effect was always below 10% of the physical broadening. The diffraction geometry was of parallel-beam type. The measurements were conducted at

about the center, half radius, and close to the edge of the samples, i.e., at positions where the shear strains were distinctly different. The X-ray line profile analyses (XPA) were applied to the measured data using the convolutional multiple whole profile (CMWP) procedure.^[39,40] Here, theoretically calculated and convoluted profile functions accounting for the crystallite size, distortions, planar defects, and instrumental effects were fitted to the measured diffraction patterns after having determined the background scattering separately. Due to the high resolution of the double-crystal diffractometer used, the instrumental effect could be neglected.

For the measurement of microhardness, the HPT discs were mechanically polished in the same way as for SEM investigations. Using a PAAR MHD microhardness tester equipped with a Vickers indenter, a load of 1.5 N was applied for 15 s, and indentations were achieved in distances of 0.5 mm along four different radial directions of the disc from the center to the edges. Samples for the macrohardness tests (with Vickers indenter) were held in liquid nitrogen all time after HPT processing, afterward mechanically polished in liquid nitrogen, and then subjected to macrohardness indentations, which were also applied in liquid nitrogen environment at a load of 49 N held for 15 s. Indentations were made from the discs' center along four directions in intervals of 0.75 mm. Subsequently, diagonals of indentations were measured at ambient temperature by optical microscopy.

The nanoindentation measurements were conducted with an ASMET UNAT nanohardness indentation facility, using a Berkovich indenter at a force of 50 mN. The nanohardness was evaluated from in situ depth measurements according to the method of Oliver and Pharr.^[41] Indentations were achieved in three rows consisting of 250 ones in each row at a distance of 20 μm in between them.

3. Results and Discussion

3.1. Mechanical Properties

The measurements of microhardness on CoCrFeNiMn alloy after HPT processing at 300 K (Figure 3a) show a significant increase, i.e., till at least three times the microhardness of the initial coarse-grained structural state, being 1.64 GPa. One of the reasons for the strong hardening may be the occurrence of twins in the beginning of the HPT processing, which strongly contributes itself both to the hardening and to the evolution of nanostructure (see Section 3.2 for measured twin density till a torsional shear strain $\gamma = 20$). Beyond $\gamma = 50$, the microhardness shows no further significant variations with increasing strain (Figure 3a). Moreover, a variation of pressure between 4 and 8 GPa of HPT processing had no significant effect on resulting microhardness values. The values of microhardness measured after HPT processing at 300 K are in good correlation with the results of all other investigations having done hardness tests in RT-HPT processing of the Cantor alloy.^[24–35]

The measurements of microhardness after HPT processing at 77 K and 6 GPa, however, gave a surprising result. At least for torsional shear strains $\gamma > 20$, they showed a lower value than that after RT-HPT processing. Such an effect was also found by

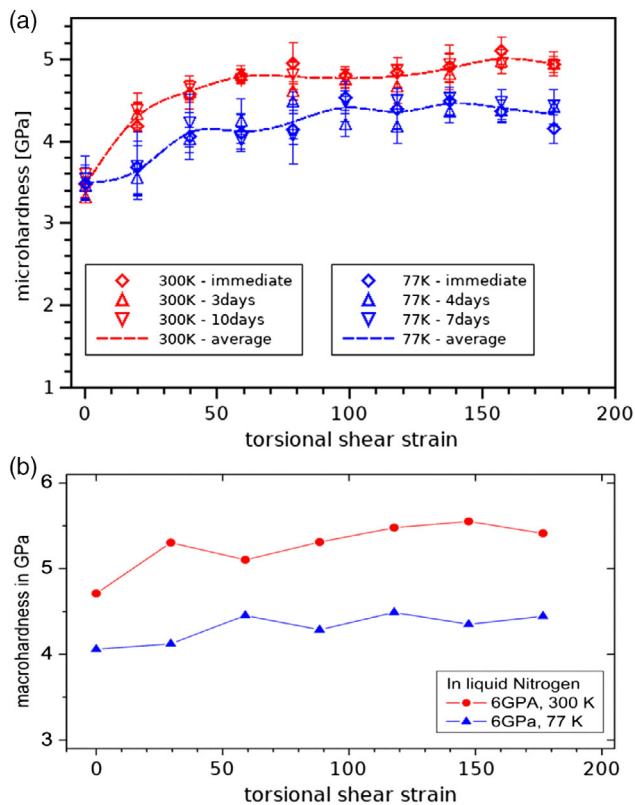


Figure 3. Hardness of CoCrFeNiMn HEA after HPT processing up to $\gamma = 180$: a) microhardness (load 1.5 N) measured at 300 K after RT-HPT processing at 6 GPa and after cryo-HPT processing at 6 GPa for various annealing times at 300 K; b) macrohardness (load 49 N) measured in liquid nitrogen at 77 K after RT-HPT processing and cryo-HPT processing, both done at 6 GPa.

Moon et al.^[30] at an HEA alloy with the same constituents but unequal percentages of them, in contrast to the equiatomic “Cantor” alloy investigated here. The effect, however, was observed to be unstable against annealing at 300 K, which meant that the low level of microhardness after cryo-HPT processing was a result of annealing-induced recovery, after having a level of microhardness higher than that of RT-HPT immediately after cryo-HPT, as it is expected from cryogenic deformation in metals and alloys. In this situation, the authors of this work undertook experiments similar to those of Moon et al.^[30] which measure the microhardness not only after long time but also after very short time of RT annealing, including data obtained immediately after HPT processing. In fact, as shown in Figure 3a, the level of microhardness measured after shorter annealing times as well as immediately after cryo-HPT was—within the measuring error—*identical* to that measured after long annealing times at 300 K, and the surprising result of microhardness level of cryo-HPT to be distinctly lower than that measured after RT-HPT has been shown to be *independent* of annealing time.

The authors also conducted macrohardness indentations under liquid nitrogen with no storage at RT between the end of HPT processing and the indentation event (Figure 3b). The results were similar to those of the microhardness tests. Apart

from a small difference in absolute values probably because of some load dependence of hardness testing, the macrohardness data showed the same paradox in strength, i.e., the strength arising from cryo-HPT processing was distinctly lower than that after RT-HPT processing, although the sample had no chance to recover before the indentation event.

The ultimate confirmation that the low strength is achieved by the cryo-HPT processing itself and does not arise from recovery effects came from torque measurements taken in situ during the HPT processing. Again, as shown in Figure 2a, the shear stress acting during cryo-HPT distinctly lies below that of RT-HPT processing, confirming the results from the hardness tests reported earlier. The wavy characteristics seen in the torque data reflect periods of full rotations and thus can be attributed to the misalignment of torsional axis of HPT setup. Also apparent in the analysis of the torque curves is that the torque of the cryo-HPT processing is higher than that of the RT-HPT processing from the beginning of the shear deformation until about $\gamma = 3$. It is interesting to note that the investigations of Stepanov et al.^[22] on Cantor alloy which has been cold rolled to $\gamma = 3$ also exhibited higher microhardness values in case of cryo-rolling than those of RT rolling. One could argue that deformation by cold rolling does not imply a high hydrostatic pressure, but a similar result was reported by a recent work of Zherebtsov et al.^[33] who tested the tensile strength of Cantor alloy after RT and cryo-HPT processing until $\gamma \approx 14$.

In this situation, it thus seemed sensible to undertake some nanoindentation investigations in frame of the current work, which appear to be more reliable than micro- and macrohardness because of their higher mechanical sensitivity and spatial resolution. Indeed, not only the paradoxical cryo-softening effect was found, but also the cross-over phenomenon, by means of the nanohardness data taken after RT and cryo-HPT processing at about $\gamma \approx 25$ (Figure 2b). Therefore, the results of the torque measurements—at least qualitatively—have been confirmed that there exists a cross-over of RT and cryogenic strength data, thus explaining why neither Stepanov et al.^[22] nor Zherebtsov et al.^[33] found the paradoxical cryo-softening effect. An interesting detail concerns the mean variance of the nanohardness values of the two HPT-processing treatments. Especially, in the region $\gamma = 25$ –50 where the cryo-softening occurs, the mean variance of the cryo-HPT processing values is about twice as large as that of the RT-HPT processing values; due to the high spatial resolution of the nanoindentation method, this result clearly reflects an increased heterogeneity in the micro/nanostructure of the cryo-HPT-processed sample. This point will be discussed again in the subsequent section dealing with the microstructural details.

3.2. Microstructure

An important result from the previous section is that according to the stability during RT storage of hardness values after RT-HPT and especially after cryo-HPT processing, it can be assumed that the microstructures connected to those strength values are stable as well. Therefore, even lengthy sample preparations and microstructural investigations conducted at RT did not change the microstructure.

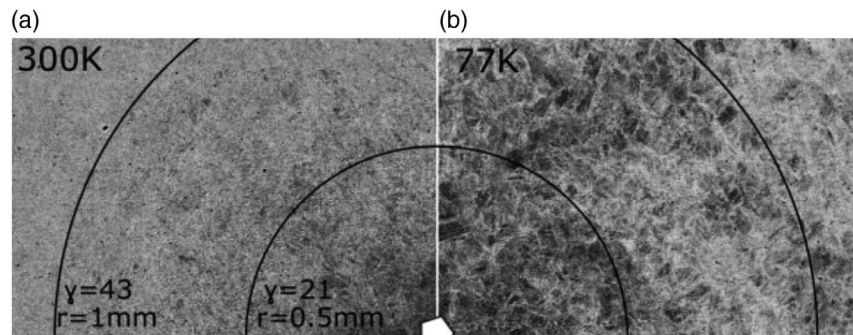


Figure 4. SEM images of HEA CoCrFeNiMn after HPT processing a) at 6 GPa, 300 K and b) at 6 GPa, 77 K, up to torsional strains $\gamma = 0, \dots, 50$; r is the distance from the center.

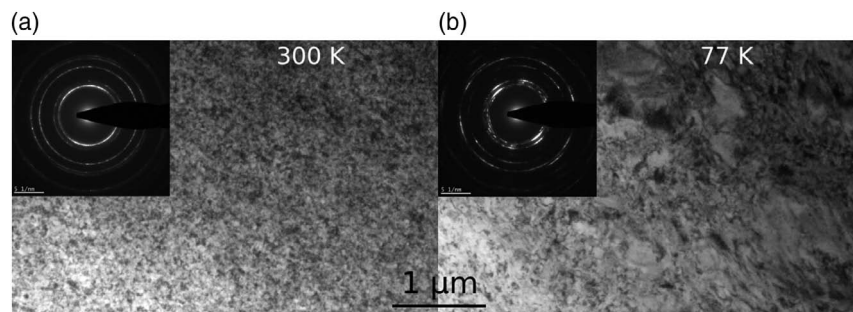


Figure 5. TEM images (bright field) of HEA CoCrFeNiMn after HPT processing at 6 GPa, 300 K a) and at 6 GPa, 77 K b), both with corresponding diffraction patterns as inserts. The value of torsional shear strain γ for both images (a,b) is 60.

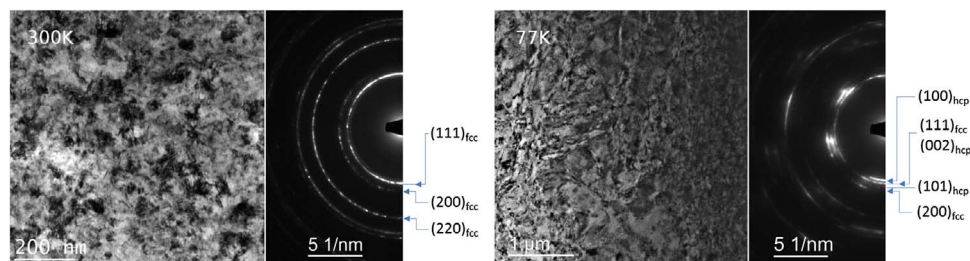


Figure 6. TEM images and SAD patterns taken from samples that were HPT-processed at a pressure of 6 GPa till torsional shear strains $\gamma = 60$. The processing temperatures were 300 K (left image) and 77 K (right image). Within the SAD patterns, the reflections of both the fcc phase and martensitic hcp phase have been indicated.

In this work, SEM and TEM investigations of the microstructure were undertaken. In the case of RT-HPT processing, a homogenous and nanocrystalline structure developed (Figure 4a, 5a, and 6) with a majority of grains with sizes between 40 and 80 nm, and very few grains with sizes larger than 200 nm (Figure 5a and 6). In contrast to RT-HPT processing, the cryo-HPT processing produced a significantly *heterogeneous* structure: along with nanocrystalline areas with grains of sizes 50–100 nm, which looks very similar to the homogeneous nanograined structure found after RT-HPT processing, larger areas with distinctly larger grains (coarse grains up to 500 nm) can also be seen (Figure 4b, 5b, and 6).

In this situation, the authors checked both the RT- and cryo-HPT-processed samples with X-ray diffraction analyses, but no evidence of a second phase and/or any change of the diffraction pattern of initial sample could be found (Figure 1a,b). That is

why the authors attempted to take the SAD patterns using TEM by which the sample diffraction area could be decreased to 1.2 μm , and thus much better localized to each of the “two phases.” Indeed, in the case of cryo-HPT SAD, in addition to the fcc reflections of nanograined area still representing the main phase, there appeared additional reflections that clearly came from the coarse-grained area, as shown in Figure 4b, 5b, and 6. In comparison with the works of Moon et al.^[29,30] and other recent ones by Tracy et al.^[42] and Zhang et al.,^[43] the new reflections are of {100} type and part of the diffraction pattern of a hexagonal close-packed (hcp) phase with the same lattice constants as the fcc phase but only a different stacking order. This suggests a martensitic transformation mechanism to have occurred here, based on the evolution of a stacking disorder along the [111] direction of the initial fcc phase.^[42] If one carefully compares the two diffractograms

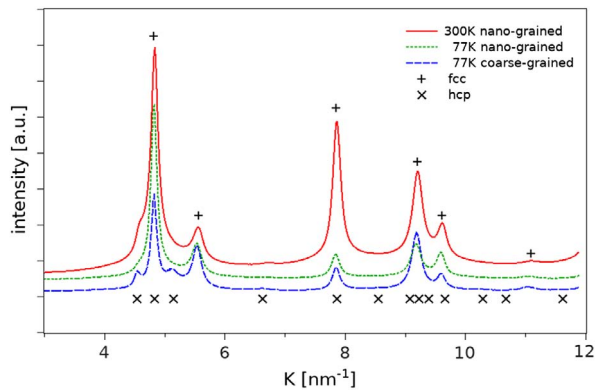


Figure 7. The diffraction patterns of reflected electron intensity versus diffraction vector K , taken from samples that were HPT-processed at a pressure of 6 GPa till torsional shear strain $\gamma = 60$, and temperatures 300 K (red curve) and 77 K (blue and green curves). The (+) symbols represent the reflections of fcc phase, whereas the (x) symbols stand for the K positions of martensitic hcp phase being identical with those from refs. [29,30,42,43], indicating a cryo-HPT-induced local-phase change. The blue curve has been obtained in selective way from the coarse-grained area shown in Figure 4b and 5b. The blue curve reflects the characteristics of the hcp phase, whereas the green curve stems from the nanocrystalline area still exhibiting the diffraction characteristics of the fcc phase.

in **Figure 7**, it seems that first traces of additional reflections also appear with the RT-HPT processing diffractogram, above all the asymmetric shoulder in the (111) peak of the fcc phase, which indicates the evolution of dislocation stacking faults as nuclei of the hcp phase. Such evidence has been found by Moon et al.^[29,30] also in case of the Cantor alloy with unequal constituent percentages, but as in the current case of RT-HPT processing, obviously the volume fraction of the hcp phase was too small to affect the strength characteristics sustainably.

3.3. Origin of the Cryo-Softening Effect: Investigations of Twin and Dislocation Density

From the measuring report and the conclusions drawn earlier, one wonders where the paradoxical softening effect in cryo-HPT-processed HEA samples comes from. At first, the sizes of grains in both phases of cryo-HPT-processed samples are found to be larger than the average grain size of the “mono-phase” RT-HPT-processed sample (for exact values of grain sizes, see Section 3.2). Already from this point of view, the lower strength of cryo-HPT-processed samples can be qualitatively explained. Because of the high defect densities to be expected in both processing routes, however, the XPA were conducted to measure the densities of dislocations and also the frequency of twins that are often formed in cryogenic plastic deformation and govern the strength and/or strengthening behavior of alloys, especially those of medium and low stacking fault energy. In SPD-processed materials, they also occur with RT as processing temperature.^[31,32] Therefore, it is not surprising that also in HEAs, especially in HPT-processed ones, twin formation has been observed, by means of TEM observations^[24] as well as of XPA measurements.^[27,28,34] **Figure 8** exhibits the results of

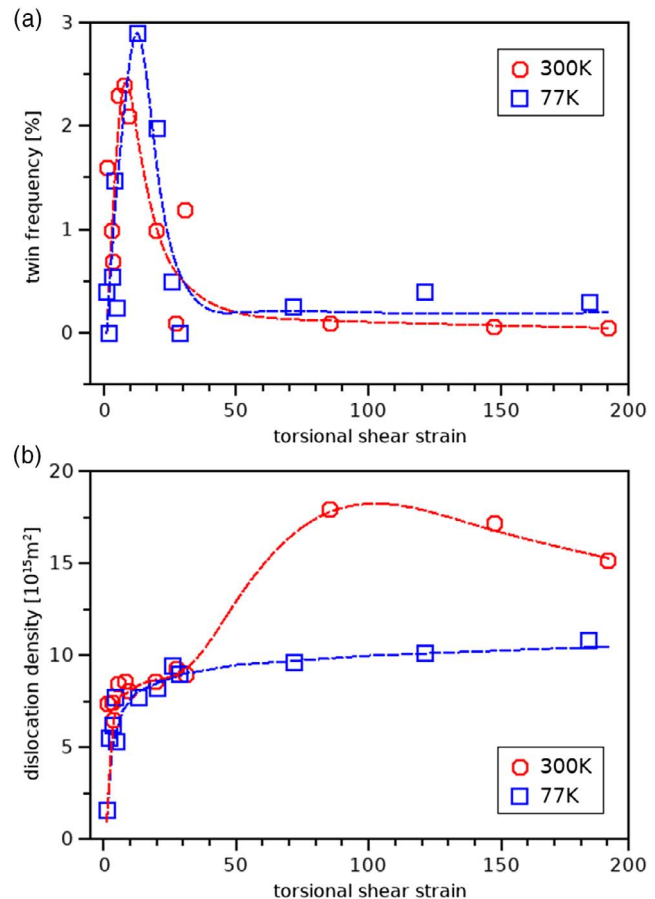


Figure 8. a) Twin frequency and b) dislocation density as measured by the X-ray line profile analysis (see text). Values indicated by red circles are measured after RT-HPT processing, and those by blue circles are measured after cryo-HPT processing. The pressure during HPT was 6 GPa. Lines are added for guiding the eyes.

the XPA analyses on the currently investigated HPT-processed samples. As in case of the direct microstructural investigations, one can trust in the results as the type and distributions of defects should not have changed significantly during storage at 300 K because of the stability of hardness values found. In **Figure 8a**, the frequency of twins, β , is presented as a function of applied torsional shear strain. As for the RT-HPT processing case, there is a strong increase in the twins' frequency until about $\beta = 2.5\%$ at $\gamma = 10$, which, however, is followed by a sharp decrease for further torsional straining until reaching almost the low level of undeformed sample, i.e., about $\beta = 0.2\%$ at $\gamma > 25$. This result agrees with the twin evidence measured by Skrotzki et al.^[28] by means of XPA and also with the results of Schuh et al.^[24] in TEM investigations. Schuh et al. observed not only a strong formation of twins at small strains till $\gamma = 2.4$, but also some development of new twin variants at higher γ 's. Nevertheless, all authors observed a dissolution of twin boundaries for $\gamma > 25$ and Schuh et al.^[24] also observed a transformation to high angle grain boundaries, thus leading to significant grain refinement. This behavior still agrees with the results found in other materials (e.g., Cu^[31,32]) with medium or low

stacking fault energy. At a shear strain $\gamma \approx 50$, a homogeneous nanograined structure was found. Surprisingly, apart from a little tendency to higher twin frequency $\beta = 0.3\%$ at $\gamma > 25$, the characteristics of twin generation and annihilation in case of the cryo-HPT processing are very similar to that of RT-HPT processing. Therefore, it cannot be made responsible for the cryo-softening effect. Nevertheless, it is interesting to note that just in the same range of shear strains $\gamma \approx 25$ – 50 where the twins disappear, the paradoxical cryo-softening sets in. In parallel to the TEM images, SAD investigations of the areas considered were done, and they showed—within the measuring error—no differences in concentration of the HEA elements between the two areas observed (Table 1); thus, any effect of concentration changes to the macroscopic strength including cryo-softening can be excluded. To make the discussion complete, it has to be noted that the texture evolutions have also been investigated in RT-HPT- and cryo-HPT-processed Cantor alloy.^[28,34] However, HPT processing strongly weakened the texture in both cases, even more in case of the cryo-HPT processing, again not providing a reasonable explanation for the cryo-softening effect.

In addition to the twin frequencies, dislocation densities could be evaluated from the broadened profiles in case of both RT and cryo-HPT processing. As a difference from the twin investigations, the dislocation densities showed a clear correlation with the strength data derived from all the hardness measurements (first similar observations were recently reported by Skrotzki et al.^[34]). At about the same strain $\gamma \approx 25$ where the strength of the two HPT-processing types start to diverge, the dislocation densities show a similar behavior than the hardness data so that one can suspect a correlation between these quantities. Indeed, following the Taylor relation that the strength is proportional to the square root of the dislocation density (the same types and arrangements of dislocations provided at different strains γ), one can estimate a strength being a factor 1.2 smaller at a torsional shear strain $\gamma \approx 50$, with an actual dislocation density difference of a factor 1.33. The actually measured strength difference is a factor 1.2, which is the same than that resulting from previous estimation. A similar agreement is found for a torsional shear strain of $\gamma \approx 100$ (factor in dislocation density equal to 1.8) where the Taylor-estimated strengths differ by a factor 1.3, whereas the measured strength values are different by a factor 1.2. A slightly worse but still good agreement is observed with the torsional shear strain $\gamma \approx 150$ where the respective factors are 1.3 for the Taylor-estimated strengths (factor in dislocation density equal to 1.6), whereas the factor between the measured hardness values is 1.1. One can conclude that practically all the strength differences within a range of torsional shear strains $\gamma = 50, \dots, 150$ can be attributed to Taylor hardening because of dislocation interaction, a result that is not unusual in HPT severely processed materials where the hardening from grain size often plays a minor role or is completely negligible.^[44]

Table 1. Energy-dispersive X-ray spectroscopy (EDS) analysis (HPT 77 K—sample): concentration of the elements (error $\approx 0.5\%$).

	Cr [at%]	Mn [at%]	Fe [at%]	Co [at%]	Ni [at%]
Heterogeneous area	20.9	19.1	20.8	20.2	19.0
Homogeneous area	20.4	20.0	20.1	20.1	19.4

In several studies (see, e.g., Li et al.^[48]), the martensitic hcp phase is made responsible for the strength being larger than that of the fcc one. However, in the present case, its fraction seems to be too small to compensate for the softening effect from the drastic decrease in dislocation density, as this one can account—for the softening alone.

It seems that a major part of dislocations (those that seem to be missing at cryo-HPT processing in comparison to RT-HPT processing) is needed to generate the new phase mentioned in Section 3.2, which then spreads over the sample volume while the dislocations disappear. For more recent literature on this phase, see refs. [45,46].

It is clear that, with the help of dislocation-mediated shear deformation, the minimum hydrostatic pressure to generate the new hcp phase by means of compression deformation solely, i.e., 14 GPa,^[42] can be reduced significantly. Very recent systematic measurements of Zhang et al.^[47] confirmed this hypothesis by showing that this critical pressure gets as small as 2–6 GPa in case of coexisting shear deformation. In principle, the situation seems to be very similar to the consequences one knows from shear-driven martensitic transformation in so-called TRIP steels. This transformation causes some extra plastic deformation, which thus decreases the stress necessary to hold on the plastic shear strain rate being a macroscopic constraint. A smaller stress—by following the Taylor relation—needs only a smaller dislocation density to operate, which was indeed measured in this article. Such an effect may also be responsible for the increase in ductility and/or fracture toughness reported in the important study of Gludovatz et al.^[7]

4. Summary and Conclusion

In this article, the so-called Cantor alloy with equal percentages of Co, Cr, Fe, Ni, and Mn has been investigated after RT and cryo-HPT processing with the following results:

- HPT processing at ambient temperature gives a uniform high-strength nanocrystalline state in CoCrFeNiMn high-entropy alloy. HPT processing at cryogenic temperatures, however, yields a bimodal microstructure of fcc and hcp phase fractions, at least with hydrostatic pressures >4 GPa and torsional shear strains $\gamma > 25$.
- At the same time, the strength falls significantly below that of the RT-HPT processing. This is true already for the strength not only during the HPT processing, but also immediately after unloading, and even after short as well as long storage times at ambient temperature of the HPT-processed HEA.
- Twins form in the beginning of HPT processing both at ambient and cryogenic processing temperatures, but disappear at the benefit of the formation of a nanocrystalline structure at torsional shear strains $\gamma > 25$.
- The small strength at cryogenic HPT processing can be understood as an indirect consequence of shear-induced phase transformation. This transformation provides a significant part of the strain necessary to hold on the macroscopic and constant rate of plastic shear deformation, thus allowing for a significant reduction of dislocation density. The reduction of Taylor hardening relation is almost equal to the

reduction in macroscopic strength so that other contributions to it appear to be negligible. This mechanism may also be responsible for literature findings of enhanced ductility and increased fracture toughness at cryogenic temperature.

Acknowledgements

A.P., Y.S., E.T., M.Z., and E.S. were supported by Austrian Agency for International Cooperation in Education and Research (OEAD GmbH), and by the Ukrainian Ministry of Education and Science, in frame of research project UA11/2017.

Conflict of Interest

The authors declare no conflict of interest.

Keywords

Cantor alloy, high-entropy alloys, high-pressure torsion, plastic deformation, cryogenic temperatures

Received: June 20, 2019

Revised: August 30, 2019

Published online: November 6, 2019

-
- [1] S. Ranganathan, *Curr. Sci.* **2003**, *85*, 1404.
- [2] B. Cantor, I. T. H. Chang, P. Knight, A. J. B. Vincent, *Mater. Sci. Eng.* **2004**, *A375–377*, 213.
- [3] C. J. Tong, Y. L. Chen, S. K. Chen, J.-W. Yeh, T. T. Shun, C.-H. Tsau, S. J. Lin, S. Y. Chang, *Metall. Mater. Trans. A* **2005**, *36*, 881.
- [4] Y. Zhang, Y. J. Zhou, *Metall. Mater. Trans.* **2007**, *561–565*, 1337.
- [5] J.-W. Yeh, Y.-L. Chen, S.-J. Lin, S.-K. Chen, *Mater. Sci. Forum* **2007**, *560*, 1.
- [6] J.-W. Yeh, S.-K. Chen, S.-J. Lin, J.-Y. Gan, T.-S. Chin, T.-T. Shum, C.-H. Tsau, S.-Y. Chang, *Adv. Eng. Mater.* **2004**, *6*, 299.
- [7] B. Gludovatz, A. Hohenwarter, D. Catoor, E. H. Chang, E. P. George, R. O. Ritchie, *Science* **2014**, *345*, 1153.
- [8] C.-W. Tsai, Y.-L. Chen, M.-H. Tsai, J.-W. Yeh, T.-T. Shun, S.-K. Chen, *J. Alloys Compd.* **2009**, *486*, 427.
- [9] J. W. Qiao, S. G. Ma, E. W. Huang, C. P. Chuang, P. K. Liaw, Y. Zhang, *Mater. Sci. Forum* **2011**, *688*, 419.
- [10] Z. Wu, H. Bei, G. M. Pharr, E. P. George, *Acta Mater.* **2014**, *81*, 428.
- [11] F. Otto, A. Dlouhy, C. Somsen, H. Bei, G. Eggeler, E. P. George, *Acta Mater.* **2013**, *61*, 5743.
- [12] A. Gali, E. P. George, *Intermetallics* **2013**, *39*, 74.
- [13] G. A. Salishchev, M. A. Tikhonovsky, D. G. Shaysultanov, N. D. Stepanov, A. V. Kuznetsov, I. V. Kolodiy, A. S. Tortika, O. N. Senkov, *J. Alloys Compd.* **2014**, *591*, 11.
- [14] M. A. Laktionova, E. D. Tabachnikova, Z. Tang, P. K. Liaw, *Low Temp. Phys.* **2013**, *39*, 630.
- [15] Y. Zhang, T. T. Zuo, Z. Tang, M. C. Gao, K. A. Dahmen, P. K. Liaw, Z. P. Lu, *Prog. Mater. Sci.* **2014**, *61*, 1.
- [16] A. D. Pogrebnjak, A. A. Bagdasaryan, I. V. Yakushchenko, V. M. Beresnev, *Russ. Chem. Rev.* **2014**, *83*, 1027.
- [17] M.-H. Tsai, J.-W. Yeh, *Mater. Res. Lett.* **2014**, *2*, 107.
- [18] E. J. Pickering, N. G. Jones, *Int. Mater. Rev.* **2016**, *61*, 183.
- [19] *Bulk Nanostructured Materials* (Eds: M. J. Zehetbauer, Y. T. Zhu), Wiley-VCH Weinheim, Germany **2009**.
- [20] A. V. Kuznetsov, D. G. Shaysultanov, N. D. Stepanov, G. A. Salishchev, O. N. Senkov, *Mater. Sci. Eng. A* **2012**, *533*, 107.
- [21] C.-W. Tsai, J.-W. Yeh, C.-C. Yang, *J. Alloys Compd.* **2010**, *490*, 160.
- [22] N. Stepanov, M. Tikhonovsky, N. Yurchenko, D. Zybkin, M. Klimova, S. Zherebtsov, A. Efimov, G. Salishchev, *Intermetallics* **2015**, *59*, 8.
- [23] M. Komarasamy, N. Kumar, Z. Tang, R. S. Mishra, P. K. Liaw, *Mater. Res. Lett.* **2015**, *3*, 30.
- [24] B. Schuh, F. Mendez-Martin, B. Völker, E. P. George, H. Clemens, R. Pippan, A. Hohenwarter, *Acta Mater.* **2015**, *96*, 258.
- [25] N. Park, X. Li, N. Tsuji, *JOM* **2015**, *67*, 2303.
- [26] a) S. Maier, *M.Sc. Thesis*, University of Vienna **2016**; b) A. Podolskiy, E. Tabachnikova, E. Schafner, C. Rentenberger, B. Joni, S. Maier, M. Tikhonovsky, A. Tortika, T. Ungar, M. Zehetbauer, presented at *Annual Meeting TMS*, Nashville, TN, USA, February 2016.
- [27] A. Heczcel, M. Kawasaki, J. L. Labar, J.-I. Jang, T. G. Langdon, J. Gubicza, *J. Alloys Compd.* **2017**, *711*, 143.
- [28] W. Skrotzki, A. Pukenas, B. Joni, E. Odor, T. Ungar, A. Hohenwarter, R. Pippan, E. P. George, *IOP Conf. Ser.: Mater. Sci. Eng.* **2017**, *194*, 012028.
- [29] J. Moon, I. H. Sun, J. W. Bae, M. J. Jang, D. Yim, H. S. Kim, *Mater. Lett.* **2017**, *202*, 86.
- [30] J. Moon, Y. Qi, E. Tabachnikova, Y. Estrin, W.-M. Choi, S.-H. Joo, B.-J. Lee, A. Podolskiy, M. Tikhonovsky, H. S. Kim, *Sci. Rep.* **2018**, *8*, 11074.
- [31] X. Z. Liao, Y. H. Zhao, Y. T. Zhu, R. Z. Valiev, D. V. Gunderov, *J. Appl. Phys.* **2004**, *96*, 636.
- [32] X. Z. Liao, Y. H. Zhao, S. G. Srinivasan, Y. T. Zhu, R. Z. Valiev, D. V. Gunderov, *Appl. Phys. Lett.* **2004**, *84*, 592.
- [33] S. Zherebtsov, N. Stepanov, Y. Ivanisenko, D. Shaysultanov, N. Yurchenko, M. Klimova, G. Salishchev, *Metals* **2018**, *8*, 123.
- [34] W. Skrotzki, presented at the European Congress and Exhibition “Materials Science Engineering”, Darmstadt, Germany, September 2018.
- [35] A. Kilmametov, R. Kulagin, A. Mazilkin, S. Seils, T. Boll, M. Heilmaier, H. Hahn, *Scr. Mater.* **2019**, *158*, 29.
- [36] A. V. Podolskiy, C. Mangler, E. Schafner, E. D. Tabachnikova, M. J. Zehetbauer, *J. Mater. Sci.* **2013**, *48*, 4689.
- [37] A. V. Podolskiy, D. Geist, E. Schafner, E. D. Tabachnikova, M. J. Zehetbauer, *IOP Conf. Ser.: Mater. Sci. Eng.* **2014**, *63*, 012071.
- [38] C. Gammer, C. Mangler, C. Rentenberger, H. P. Karnthaler, *Scr. Mater.* **2010**, *63*, 312.
- [39] L. Balogh, G. Ribarik, T. Ungar, *J. Appl. Phys.* **2006**, *100*, 023512.
- [40] M. B. Kerber, M. J. Zehetbauer, E. Schafner, F. C. Spieckermann, S. Bernstorff, T. Ungar, *JOM* **2011**, *63*, 61.
- [41] W. C. Oliver, G. M. Pharr, *J. Mater. Res.* **2004**, *19*, 3.
- [42] C. L. Tracy, S. Park, D. R. Rittman, S. J. Zinkle, H. Bei, M. Lang, R. C. Ewing, W. L. Mao, *Nat. Commun.* **2017**, *8*, 15634.
- [43] F. Zhang, Y. Wu, H. Lou, Z. Zeng, V. B. Prakapenka, E. Greenberg, Y. Ren, J. Yan, J. S. Okasinski, X. Liu, Y. Liu, Q. S. Zeng, Z. Lu, *Nat. Commun.* **2017**, *8*, 15687.
- [44] B. Jóni, E. Schafner, M. Zehetbauer, G. Tichy, T. Ungár, *Acta Mater.* **2013**, *61*, 632.
- [45] Q. Lin, J. Liu, X. An, H. Wang, Y. Zhang, X. Liao, *Mater. Res. Lett.* **2018**, *6*, 236.
- [46] P. Yu, L. Zhang, H. Cheng, H. Tang, J. Fan, P. K. Liaw, G. Li, R. Liu, *J. Alloys Compd.* **2019**, *779*, 1.
- [47] F. Zhang, H. Lou, S. Chen, X. Chen, Z. Zeng, J. Yan, W. Zhao, Y. Wu, Z. Lu, Q. Zeng, *J. Appl. Phys.* **2018**, *124*, 115901.
- [48] Z. Li, K. G. Pradeep, Y. Deng, D. Raabe, C. C. Tasan, *Nature* **2016**, *534*, 227.